Gold in Ores of the Natalka Giant Deposit (North East Russia): Content, Distribution and Speciation

R. G. Kravtsova[1] , A. S. Makshakov[*,1] , V. L. Tauson[1] , S. V. Lipko[1] , and O. Yu. Belozerova[1]

[1]Vinogradov Institute of Geochemistry, Siberian Branch of the Russian Academy of Sciences, Irkutsk, Russia
* **Correspondence to:** Artem Makshakov, artem_m@mail.ru.

Abstract: The content, distribution and speciation of gold in ores of the Natalka deposit (North East Russia) were studied. According to atomic absorption spectrometry (AAS), the vein and veinlet-vein ores are highest grade in gold, whereas veinlet-disseminated ores are lower grade and disseminated ores are poor in gold. According to light microscopy and electron probe microanalysis, up to 85% of gold in the Natalka ores is represented by large and small grains of free native gold associated with gangue and sulfide minerals. The gold grains of 0.01 to 2 mm in size are dominated and their fineness vary from 720 to 860 ‰. Up to 20% of native gold is represented by finely dispersed particles < 0.01 mm in size and a fineness of 750–990‰. Most of this gold is fixed and bounded mainly to with sulfides. According to "phase" chemical analysis with AAS, arsenopyrite is richest in gold whereas pyrite is poorer in gold. Using AAS with analytical data selections for single crystals, two non-mineral forms of "invisible" gold were found in these sulfides, namely the structurally bound (structural) and surficially bound (surficial) forms. The structural gold is incorporated into the mineral structure. The surficial form is confined to nano-sized non-autonomous phases on the sulfide mineral surfaces and often dominates over the structural form. The maximum gold concentrations on the surface of arsenopyrite and pyrite were confirmed by LA-ICP-MS data. It is expected that not all "invisible" gold is a refractory gold. The major part of gold contained in arsenopyrite and pyrite as finely dispersed, micron- and submicron-sized particles, as well as the surficially bound gold, can be extracted with modification of current flowsheet, which enhances the value of the gold ores at the Natalka deposit.

Keywords: Natalka deposit, gold, ores, content, distribution, gangue minerals, sulfide minerals, arsenopyrite, pyrite, speciation.

1. Introduction

The territory of North East Russia is known to be the largest auriferous province that is unique in terms of the count of gold deposits, many of which have no analogies either in Russia or abroad. The Natalka giant gold deposit is one of the most striking examples. Previous studies of the ore material composition of this deposit typically focused on the native gold, most of which, is known to be in "free" form as the intergrowths and inclusions (0.01 to 2.0 mm in size) in gangue (mainly quartz) and sulfide minerals [*Goncharov et al.*, 2002; *Goryachev et al.*, 2000; *Savva et al.*, 2022].

The study of ores and genesis of such deposits and, as a result, the assessment of their commercial significance usually begins with the characterization of typical features of large- and small-size gold. Less attention is paid to the problem of studying finely dispersed (<10 μm) native gold and, so-called, "invisible" gold. Most of this gold is fixed. Numerous papers have shown that the study of such gold is extremely in demand when identifying the composition of ores, mineralization stages, conditions of mineral formation

and, in general, the genesis of gold deposits [e.g., *Barker et al.*, *2009*; *Cabri et al.*, *1989*; *Cambel et al.*, *1980*; *Cook and Chryssoulis*, *1990*; *Ehrig et al.*, *2023*; *Fleet and Mumin*, *1997*; *Gao et al.*, *2019*; *Genkin et al.*, *1998*; *Koneev et al.*, *2020*; *Kravtsova*, *2010*; *Kravtsova and Solomonova*, *1985*; *Kravtsova et al.*, *2022*; *Large and Maslennikov*, *2020*; *Large et al.*, *2009*; *Liu et al.*, *2019*; *Moiseenko and Kuznetsova*, *2010*; *Morishita et al.*, *2018*; *Moskvitin et al.*, *2023*; *Palenik et al.*, *2004*; *Shao et al.*, *2018*; *Sidorova et al.*, *2020, 2022*; *Simon et al.*, *1999*; *Tan et al.*, *2022*; *Tauson et al.*, *2013*; *Wells and Mullens*, *1973*; *Zhang et al.*, *2014*; *Zhao et al.*, *2011*].

Only some papers contain information on the distribution of finely dispersed and "invisible" gold in ores and minerals of the Natalka deposit [*Goncharov et al.*, *2002*; *Kravtsova et al.*, *2015, 2022*; *Plyusnina et al.*, *2003*; *Volkov et al.*, *2006*]. According to the rational analysis of ores given in [*Goncharov et al.*, *2002*], the amount of such gold usually does not exceed 14.2% and is mostly associated with sulfides, mainly with arsenopyrite and pyrite. Its losses during extraction from sulfide concentrates are unavoidable and often significant. According to [*Goryachkin et al.*, *1999*], during the auriferous raw material beneficiation, under the current flowsheet at the Natalka deposit, the losses of this metal in the sorption tailings of sulfide concentrates reach 3.8 g/t, which is commensurable with the contents in ordinary ores (2.5 to 5.0 g/t) and amount up to 30% of the total gold (8.03 g/t) in these concentrates. For the Natalka deposit, which is relatively simple in terms of beneficiation technology, such losses are very appreciable.

The gold lost during raw material processing together with the sulfide component is mainly micron, submicron and "invisible". Ores containing such gold are considered to be "refractory", requiring the use of special flowsheets. The study of its speciation is directly related to such flowsheets, since it significantly affects the technological features of ores and, as a result, the methods of their beneficiation. These features can already be established at the early stages of the deposit research when studying both the native gold (from its large particles to micron and submicron 1 μm and less in size), and its "invisible" forms, which are difficult for recovering.

Our comprehensive approach to carry out such investigations has yielded good results. In addition to the gold content and distribution, coarseness and fineness, impurities, mineral associations, etc., special attention was paid to the detailed study of the composition of finely dispersed gold inclusions (primarily micron and submicron-sized) and the species of so-called "invisible" gold. In ores of the Natalka deposit, the concentrators of such gold are arsenopyrite and pyrite. The need for such research is important, not only for studying the genesis of gold deposits. Finding out the reason for the loss of refractory gold contained in sulfide concentrates during ore processing and the use of the results obtained in practice are also much-in-demand.

2. Research objects

The Natalka deposit, the ores of which are the object of our research, is one of the largest gold deposits in Russia. It is located in the Tenka district of the Magadan region in North East Russia (Figure 1, inset). The deposit belongs to the orogenic sulfide-poor type. It has a complicated and long-term development history and a metamorphogenic-hydrothermal genesis. According to most researchers, magmatic fluids took an active part in the ore formation [*Goncharov et al.*, *2002*; *Goryachev et al.*, *2008*; *Mikhalitsyna and Sotskaya*, *2020*; *Savva et al.*, *2022*; *Volkov et al.*, *2016*].

Late Permian carbonaceous terrigenous rocks host ores. They include siltstone shale, argillaceous siltstone and sandstone of the Omchak Formation, diamictite (argillaceous and siltstone shale with an admixture of volcanic clastic material of various sizes) of the Atka Formation, carbonaceous-argillaceous and siltstone shale, argillaceous siltstone, sandstone and gravelstone of the Pioneer Formation (Figure 1). The ore lode in the silicified sedimentary strata (mainly diamictite, siltstone and siltstone shale), traced along the strike for a distance of about 4–5 km and with a width of 100–600 m, represents only a smaller part of the mineralized zone (Figure 1). The lode consists mainly of quartz veins, a net of branching or parallel veins and veinlets and areas of disseminated sulfide mineralization

in the host rocks [*Grigorov et al.*, 2007]. The highest grade gold ores include vein and veinlet-vein ores, the lower grade are veinlet-disseminated ores and the poor ones are disseminated ores (Figure 2).

In vein and veinlet-vein ores (Figure 2a, b) of the late hydrothermal stages of ore formation, gangue minerals are quartz, carbonate, sericite, albite and K-feldspar. The proportion of ore minerals, mainly sulfides, does not exceed 3%. The most common are arsenopyrite and pyrite. Galena, chalcopyrite and sphalerite are less common and pyrrhotite, ilmenite, rutile, scheelite, fahlores and native gold are even rarer. According to [*Goncharov et al.*, 2002], rare occurrences of boulangerite, bournonite, acanthite and stibnite are also found. Fragments of host rock from breccia-like quartz veins contain carbonaceous matter and graphite microflakes, which impart to the fragments color ranging from dark gray to black (Figure 2b). Visible gold is often met (Figure 2a, b).

Veinlet-disseminated ores (Figure 2c) of the early hydrothermal stage are represented by quartz and carbonate-quartz veinlets in carbonaceous diamictite, less often in siltstone and siltstone shale. The proportion of sulfide minerals is higher here, up to 5%. As for the ore minerals, arsenopyrite and pyrite are relatively common; less common are chalcopyrite, pyrrhotite, ilmenite, rutile and scheelite. Single graphite microflakes and small aggregates of weakly metamorphosed carbonaceous matter are found in the rocks hosting the veinlets. Visible gold is rare.

Disseminated ores (Figure 2d) of the initial metamorphogenic stage are the part of the ore lode and the entire mineralized zone. The latter are represented by zones of disseminated sulfide mineralization (ZDSM) in carbonaceous diamictite, siltstone and siltstone shale. Sulfides amount less than 3% and represented mainly by pyrite and rarely arsenopyrite. No visible gold was found. Most rocks are impregnated with rare, finely dispersed inclusions of graphite microflakes and carbonaceous matter. The disseminated ores of mineralized zone are not currently of practical interest, despite the fact that this zone is significantly larger in size than the lode (Figure 1).

A complete description of the ore composition and formation conditions of the Natalka deposit is given in [*Goncharov et al.*, 2002] and supplemented by later papers [*Goryachev et al.*, 2008; *Goryachkin et al.*, 1999; *Kravtsova et al.*, 2015, 2022; *Mikhalitsyna and Sotskaya*, 2020; *Plyusnina et al.*, 2003; *Savva et al.*, 2022; *Volkov et al.*, 2006].

3. Materials and Methods

To determine gold content, distribution features and speciation in ores and sulfide minerals, 75 large-volume mineralogical-geochemical samples were taken in different areas and horizons of the deposit. These samples were analyzed for gold using atomic absorption spectrometry (AAS), based on the extraction of gold from solution by organic sulfides. Measurements of the Au content were carried out on the Perkin-Elmer M503 device (USA) with a graphite atomizer furnace HGA-72. The detection limit of gold determination is 0.3 ppb [*Method NSAM No. 237-S*, 2016].

Along with light microscopy (LM), the method of X-ray electron probe microanalysis (EPMA) was used when investigating mineral and chemical composition of ores, to study the typical features of native gold, its size, fineness, trace elements, internal structure, mineral associations, micro and finely dispersed inclusions in arsenopyrite and pyrite crystals [*Pavlova*, 2014]. The polished sections of ore samples were examined using a scanning electron microscope mode on the electron probe microanalyzer Superprobe JXA-8200 (JEOL Ltd., Japan). The determination of the chemical composition of the found gold particles available in the form of inclusions and micro-inclusions (>3 µm in size) in quartz and sulfide minerals, was performed by monitored acquisition, recalculating the recorded relative intensities in concentration using the microanalyzer software. The determination of the basic composition, i.e., the fineness of micron (1 to 3 µm) and submicron-sized (<1 µm) inclusions of native gold in arsenopyrite and pyrite, was implemented according to a specially developed EPMA procedure [*Finkelshtein et al.*, 2018], which gave an option of eliminating the sulfide matrix influence on the determination of Au and Ag contents.
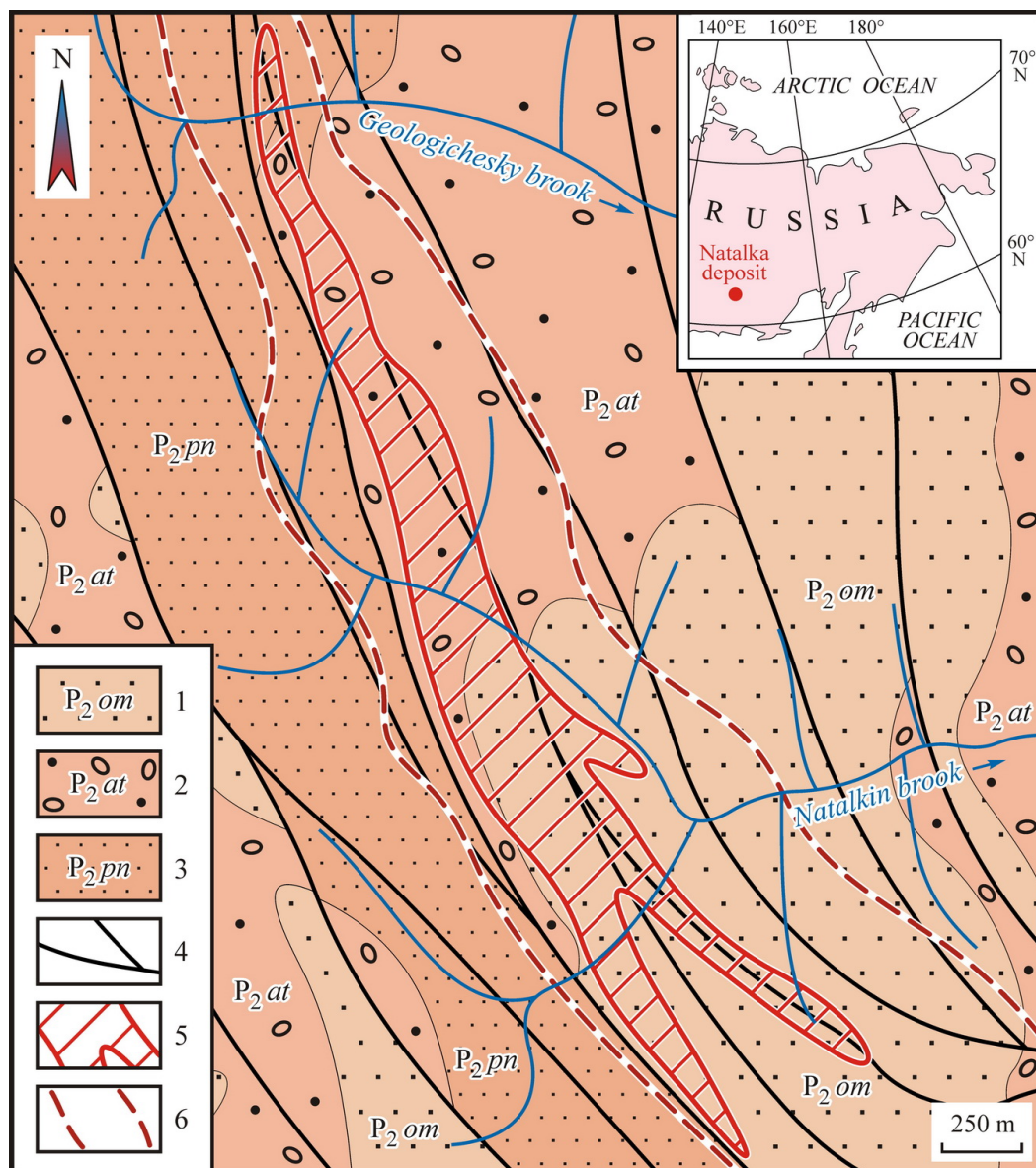
Figure 1. The schematic geological map of the Natalka gold deposit. Constructed by the authors using the data [*Goncharov et al.*, 2002; *Grigorov et al.*, 2007] and materials from geological funds of the "Matrosov mine" public corporation (Magadan, Russia). 1–3 – Late Permian ore hosted terrigenous rocks: 1 – siltstone shale, argillaceous siltstone and sandstone of the Omchak Formation (P_2om), 2 – diamictite of the Atka Formation (P_2at), 3 – carbonaceous-argillaceous and siltstone shale, argillaceous siltstone, sandstone and gravelstone of the Pioneer Formation (P_2pn); 4 – faults; 5 – ore lode projection; 6 – conventional boundaries of the mineralized zone.

The procedure is based on the extrapolation of relation between element contents in the inclusion and matrix into the area where the matrix element content tends to zero. The measurements were also implemented applying the Superprobe JXA-8200 device (microanalyzer). More than 350 measurements were taken to study the chemical composition of gold.

To study the total content of Au in monomineral samples of arsenopyrite and pyrite, which contained both crystals and their aggregates with different sizes and shapes, "phase" chemical analysis with AAS (PCA-AAS) was used. The Au content determination was carried out on one test charge or in parallel, on two test charges (15 to 20 mg each) of different size fractions. The abraded material was decomposed with aqua regia under
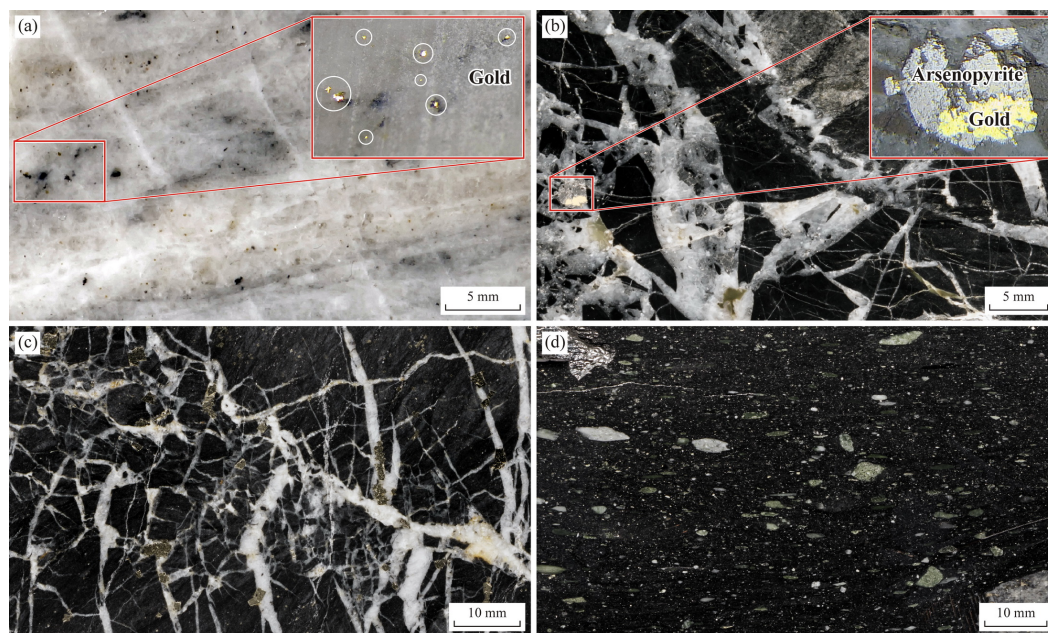
Figure 2. Ore types in the Natalka gold deposit: (a) – vein (massive quartz vein with a small amount of fragments of hosting siltstone, with nests and inclusions of arsenopyrite and visible gold); (b) – veinlet-vein (breccia-like quartz vein, quartz and carbonate-quartz veinlets in carbonaceous siltstone with nests and crystals of arsenopyrite, pyrite and visible gold); (c) – veinlet-disseminated (carbonaceous-argillaceous siltstone dissected by quartz and carbonate-quartz veinlets with arsenopyrite and pyrite); (d) – disseminated (carbonaceous diamictite with fragments of different composition and dimensions with fine pyrite inclusions).

heating. It was then treated with concentrated HCl and evaporated dry to remove nitric acid residues and convert the salts to the chloride form. After cooling, the samples were brought to a certain volume with a background solution of 2M HCl for measurements using AAS method on the Perkin-Elmer M503 device with detection limit for gold of 0.3 ppb and an accuracy of 12% [*Tauson et al.*, 2002].

The speciation of "invisible" gold in the arsenopyrite and pyrite of the Natalka deposit was studied using AAS with analytical data selections for single crystals (AAS-ADSSC). The method developed by V. L. Tauson and co-authors [*Tauson and Lustenberg*, 2008; *Tauson et al.*, 2002] is based on rank-scaled statistical sampling of analytical data for a large number of individual crystals of one and the same mineral sample, to separate the structurally and surficially bound forms of impurity elements. Euhedral crystals with well-defined morphology were selected from monomineral fractions of different sizes, from 0.2 to 2.0 mm. The crystals did not contain any visible mineral inclusions. The crystals of arsenopyrite were shaped as pseudo-orthorhombic and monoclinic prisms. The crystals of pyrite generally had the shape of a cube or parallelepiped. The samples complicated by the facets of pentagonal dodecahedron and octahedron were excluded whenever possible. The requirement for the shape is due to the fact that in the transition from size to specific surface area of average crystal in size selection it is necessary to use the form coefficient for the true polyhedron. In our case, the coefficient was six for cubes and parallelepipeds. The Au content is determined in solutions obtained through the acidic decomposition of well-faceted individual crystals of arsenopyrite and pyrite. The AAS-ADSSC technique is designed to determine the content of the structurally and surficially bound trace elements (in our case, Au) in the samples consisting of individual crystals with an uncertainty of ±30 rel. % [*Tauson and Lustenberg*, 2008; *Tauson et al.*, 2013]. The data obtained were statistically processed according to the regularities of the distribution of different species of the element [*Tauson and Lustenberg*, 2008; *Tauson et al.*, 2018a].

The study of Au content in the surface layer of arsenopyrite and pyrite crystals was continued using the LA-ICP-MS method. A quadrupole inductively coupled plasma mass spectrometer NexION 300D (Perkin-Elmer, USA) was used in combination with a laser ablation system NWR-213 (New Wave Research, USA). The working and carrier gases were Ar and He, at 99.999% purity. The laser burned continuous grooves (tracks) on the natural surface of the crystals. The track lengths were limited by the size of the crystal faces and varied in the range of 0.3–1.0 mm. The diameter of the laser beam was 100 μm, the frequency – 10 Hz, the energy on the surface of the sample – 0.4 J/cm^2, the laser speed – 70 μm/s and the background measuring time – 20 s. The track depth per one laser pass for all sulfide crystals was ~1.0 μm. The depth was measured using atomic force microscopy with SMM-2000 scanning probe microscope (Proton-MIET, Russia). The calibration graphs were constructed in compliance with the NISTSRM610, NISTSRM612, NISTSRM614, BHVO-2G, TB-1G and NKT-1G international standards. It was possible to verify the results for Au using the in-house sulfide reference sample – highly homogeneous ferrous greenockite (α-CdS) crystals synthesized hydrothermally at 500 °C and 1 kbar pressure [*Tauson et al.*, 2019]. The instrument error determined for Au did not exceed 10%.

4. Results

4.1. Content and distribution of gold

According to the AAS data, the highest grade vein and veinlet-vein ores are characterized by high average Au content: 29.2 ppm (within the range of 0.39–109.1 ppm) and 27.2 ppm (0.38–106.9 ppm), respectively. For the lower grade veinlet-disseminated ores, less high Au content is common, on average 1.33 ppm (within the range of 0.45–2.90 ppm). For the poor, so-called disseminated ores, which are part of the ore lode and the ZDSM, the average Au content is 0.11 ppm (within the range of 0.05–0.6 ppm) and 0.08 ppm (0.02–0.19 ppm), respectively.[1]

The Au content and distribution in arsenopyrite and pyrite of the Natalka deposit were studied using PCA-AAS. These sulfides were taken from samples consisting of monomineral fractions with different grain sizes. The results of summarizing the available and newly obtained data are shown in Table 1. The highest average Au contents (ppm) were found in arsenopyrite monofractions: from vein – 626.1 (within the range of 3.3–1383), veinlet-vein – 42.5 (4.3–119.0), veinlet-disseminated – 30.2 (1.4–55.2) and disseminated ores of the lode – 3.1 (2.5–3.8). Lower average Au contents (ppm) were found in pyrite monofractions: from vein – 70.5 (within the range of 11.3–250.1), veinlet-vein – 8.5 (1.3–17.9), veinlet-disseminated – 4.6 (0.5–18.1) and disseminated ores of the lode and ZDSM – 2.9 (2.1–3.4) and 1.1 (0.8–1.7), respectively.

4.2. Gold speciation

4.2.1. Native gold in ores and minerals

According to our mineralogical studies (LM and EPMA methods), up to 85% of gold in the vein, veinlet-vein and veinlet-disseminated ores is represented by large and small grains of free native gold. It is associated with gangue minerals, primarily quartz and feldspars (Figures 3, 4b, c, 5c), and with sulfide minerals such as arsenopyrite, pyrite, chalcopyrite, galena, sphalerite, less often pyrrhotite and tetrahedrite (Figures 4–7). The native gold–arsenopyrite association is the most typical for the ores of the Natalka deposit (Figures 4c, 5). Gold grains of 0.01 to 2.0 mm in size are prevalent. Structural etching reveals a homogeneous polygonal-granular structure of gold with simple twins. Various gold forms were observed: isometric, slightly elongated, vein-like, lumpy and partially faceted, with crystal-like outgrowths. According to the EPMA, the fineness of the studied gold is 720–860‰. The qualitative and quantitative composition of the inherent impurity elements in native gold, established by the same method, is relatively poor. The impurities

---

[1] Number of samples for vein, veinlet-vein, veinlet-disseminated and disseminated ores equaled 20, 20, 20 and 15, respectively.

Table 1. Gold content in the monomineral fractions of arsenopyrite and pyrite of different sizes from various ore types of the Natalka deposit. PCA-AAS data

Sample No.	Ore type	Brief description of the samples from which sulfides were taken	C_{int} (ppm)	C_{av} (ppm)	N (n)
		Arsenopyrite			
M-129/10	V	Massive quartz vein with inclusions, mainly arsenopyrite	46.5–141.1	93.8	3 (3)
M-129/10-2	V	Quartz vein with rare fragments of diamictite and inclusions of arsenopyrite, rarely pyrite	3.3–310.1	91.8	3 (4)
M-161/10	V	Massive quartz vein with inclusions of arsenopyrite, less often pyrite	19.1–1383	626.1	4 (5)
M-131/10	VV	Carbonate-quartz veins and veinlets in diamictite with arsenopyrite inclusions	6.2–84.9	32.7	4 (4)
M-131/10-2	VV	Quartz veins and veinlets in diamictite with inclusions, mainly arsenopyrite	4.3–119.0	42.5	4 (8)
G-9/13	VV	Carbonate-quartz veins and veinlets in diamictite with arsenopyrite inclusions	11.3–24.0	15.4	4 (4)
G-9/13-2	VV	Quartz veins and veinlets in diamictite with inclusions, mainly arsenopyrite	6.6–117.2	39.8	5 (5)
TPM-1/1	VV	Quartz veins and veinlets in diamictite with inclusions of pyrite, less often arsenopyrite	9.7–53.3	26.3	4 (5)
Nat-10	VD	Diamictite with a rare net of quartz veinlets with inclusions of pyrite and arsenopyrite	1.4–7.4	3.8	2 (3)
Nat-10-2	VD	Diamictite with a dense net of quartz veinlets with inclusions of pyrite, less often arsenopyrite	2.7–55.2	30.2	3 (3)
UV-3/13	VD	Diamictite with quartz veinlets and streaks and inclusions of pyrite, less often arsenopyrite	8.1–37.2	23.2	3 (3)
VK-2/10	D	Silicified siltstone from the ore lode with inclusions of pyrite, less often arsenopyrite	2.5–3.8	3.1	3 (4)
		Pyrite			
M-161/10	V	Massive quartz vein with inclusions of arsenopyrite, less often pyrite	15.3–158.2	65.4	4 (4)
M-161/10-2	V	Quartz vein with rare fragments of diamictite and inclusions, mainly pyrite	11.3–250.1	70.5	4 (6)
TPM-1/1	VV	Quartz veins and veinlets in diamictite with inclusions of pyrite, less often arsenopyrite	1.9–17.9	8.5	3 (4)
TPM-1/2	VV	Quartz-carbonate veins and veinlets in diamictite with pyrite inclusions	1.3–16.5	7.4	4 (4)
Nat-10	VD	Diamictite with a rare net of quartz veinlets with inclusions of pyrite and arsenopyrite	1.2–4.6	2.6	4 (4)
Nat-10-2	VD	Diamictite with a dense net of quartz veinlets with inclusions of pyrite, less often arsenopyrite	0.5–18.1	3.5	5 (10)
UV-3/13	VD	Diamictite with quartz veinlets and streaks and inclusions of pyrite, less often arsenopyrite	0.8–6.6	4.6	3 (3)
VK-2/10	D	Silicified siltstone from the ore lode with inclusions of pyrite, less often arsenopyrite	2.1–3.4	2.9	3 (3)
VK-2/10-2	D	Slightly altered siltstone shale from the ZDSM with pyrite inclusions	0.8–1.7	1.1	4 (6)

Notes: Here and in Table 2 and 3: V – vein, VV – veinlet-vein, VD – veinlet-disseminated, D – disseminated ore types. C_{int} is the interval of Au contents in samples (weight 15–20 mg) consisting of monomineral fractions of arsenopyrite and pyrite of different sizes represented by aggregates, crystals of different morphological forms and their combinations; C_{av} is the average Au content in samples; N is the number of analyzed samples (n is the number of measurements).

in gold wt. %), in addition to Ag (10 to 28), are often Fe (0.17 to 2.34) and S (0.10 to 0.91), less common are Bi (0.32 to 1.02), As (0.16 to 0.90), Hg (0.23 to 0.87), Cu (0.28 to 0.86) and Se (0.46 to 0.59), and at single points – W (0.24, 0.37) and Pb (0.36).

According to the data, we obtained with the same LM and EPMA methods, up to 20% of gold are finely and ultra-dispersed particles (<0.01 mm in size) of native gold. They are both free and fixed. Fixed native gold predominates and is mostly included in sulfide minerals, primarily arsenopyrite (Figures 5a, b, 8) and pyrite (Figures 6a, b, 7). Such gold does not exhibit visible crystalline forms. It usually fills the space between the crystals of these sulfides or occupies crystal defects. The fineness of finely dispersed inclusions is higher compared to large and small gold (Figure 5b, c). According to the EPMA, the fineness of the finely dispersed gold is 750–990‰.
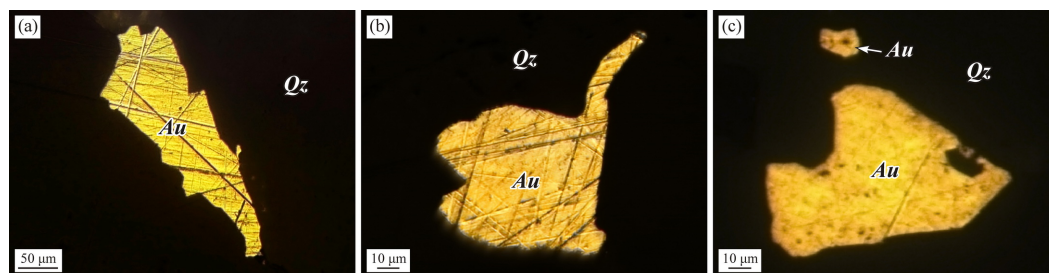
Figure 3. Native gold in association with quartz. Images are given in reflected light. Here and hereafter, *Au* – gold, *Qz* – quartz.
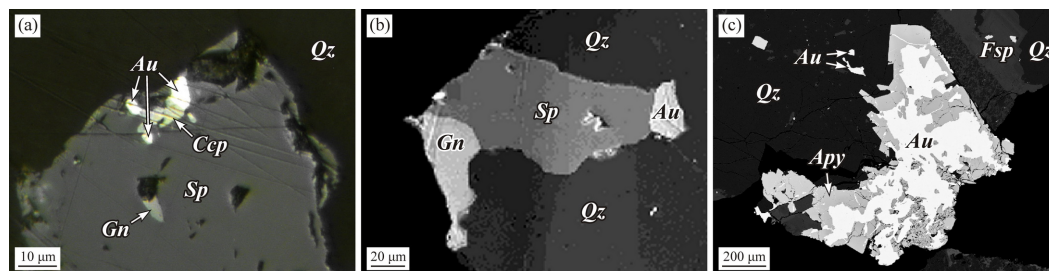
Figure 4. Native gold in association with ore minerals: (a) – inclusions of gold, chalcopyrite and galena in sphalerite; (b) – inclusions of galena, sphalerite and gold in quartz; (c) – intergrowths of gold with arsenopyrite and gangue minerals (quartz and K-feldspar). Images are given in reflected light (a), secondary (b) and backscattered (c) electrons. Here and hereafter, *Sp* – sphalerite, *Gn* – galena, *Ccp* – chalcopyrite, *Apy* – arsenopyrite, *Fsp* – K-feldspar.
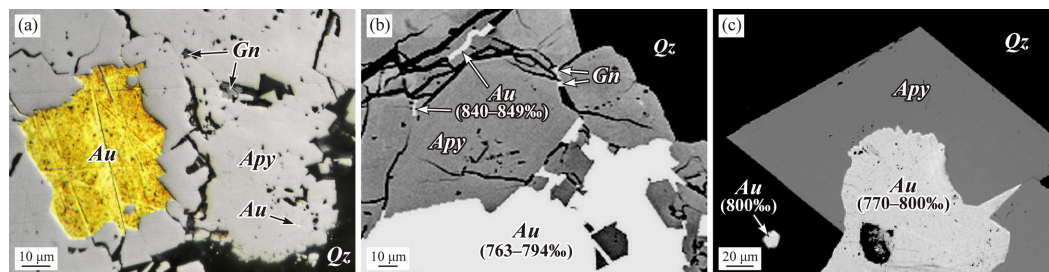
Figure 5. Large, small and finely dispersed native gold in association with arsenopyrite: (a) and (b) – inclusions of galena and gold in arsenopyrite; (c) – gold in association with arsenopyrite crystals and quartz. In parts (b) and (c) the gold fineness is indicated in parentheses. Images are given in reflected light (a) and backscattered electrons (b and c).
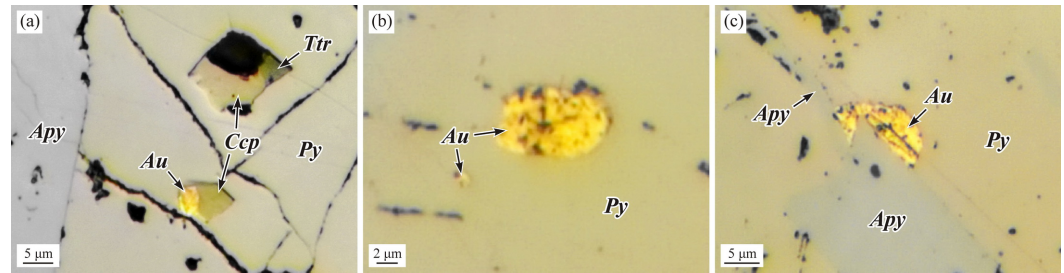
Figure 6. Native gold in pyrite: (a) – gold, chalcopyrite, Ag-bearing tetrahedrite and arsenopyrite in pyrite; (b) – finely dispersed and micron gold inclusions in pyrite; (c) – inclusions of gold and arsenopyrite crystals in pyrite. Images are given in reflected light. Here and hereafter, *Py* – pyrite, *Ttr* – tetrahedrite.
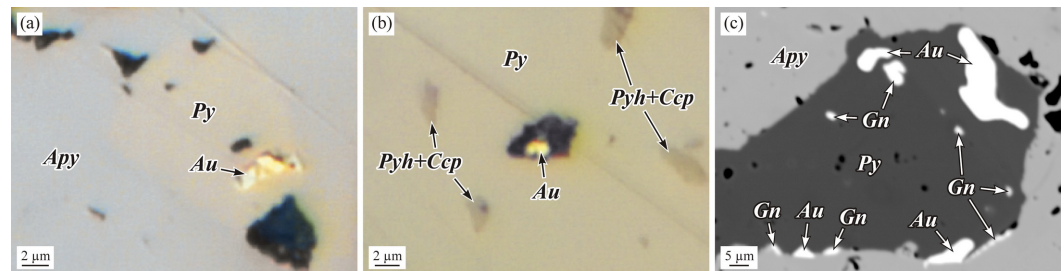
Figure 7. Inclusions of finely dispersed and small native gold in pyrite: a – gold in a pyrite crystal embedded in arsenopyrite; (b) – gold inclusion in a pyrite cavity; (c) – numerous inclusions of gold and galena in a pyrite crystal embedded in arsenopyrite. Images are given in reflected light (a and b) and backscattered electrons (c). *Pyh* – pyrrhotite.
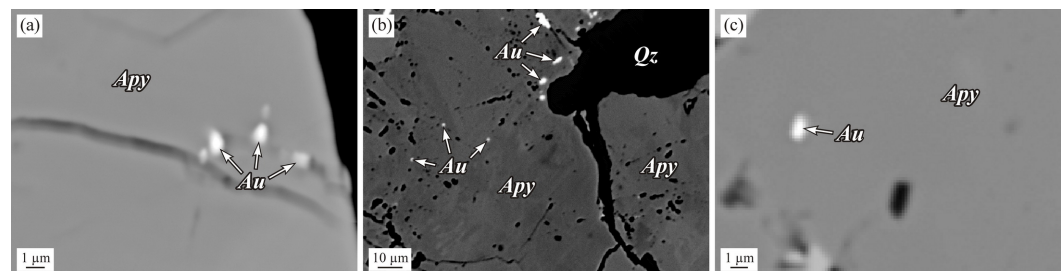
Figure 8. Inclusions of finely and ultra-dispersed gold in arsenopyrite. Images are given in backscattered electrons.

4.2.2. "Invisible" gold in arsenopyrite and pyrite

Using the AAS-ADSSC method, the concentration levels and species of the "invisible" gold in arsenopyrite and pyrite crystals were studied. The crystals of these sulfides were taken from samples consisting of monomineral fractions of arsenopyrite and pyrite of different sizes, which were previously analyzed by PCA-AAS for Au. The results of the generalization of the available and newly obtained data are shown in Table 2.

Two non-mineral species of "invisible" uniformly distributed gold were found in arsenopyrite and pyrite: structural and surficial (Table 2). The structural form corresponds to a chemically-bound element in the mineral structure; the predominant surficial form is confined to nano-sized non-autonomous phases (NAPs) and exists in a surface layer of the crystal. The proportions of the last form of the total content of "invisible" gold in arsenopyrite and pyrite from vein and veinlet-vein ores range from 81.8% to 99.9% and from 90.4% to 98.1%, respectively. These proportions are slightly lower in sulfides from veinlet-disseminated and disseminated ores sampled from silicified siltstone in the ore lode. They are from 61.3% to 96.8% and from 44.0% to 95.7% in arsenopyrite and pyrite, respectively. The smallest proportions of the surficial form of gold are typical for

Table 2. The content of "invisible" gold in arsenopyrite and pyrite crystals from various ore types of the Natalka deposit. AAS-ADSSC data

Sample No.	Ore type	Au (ppm)				P_{sur} (%)
		C_{int}	C_{av}	C_{str}	C_{sur}	
Arsenopyrite						
M-129/10	V	24.1–141 (26)	55.9	6.77	30.43	81.8
M-129/10-2	V	15.0–140 (41)	62.5	3.35	30.85	90.2
M-161/10	V	2.3–20.1 (24)	18.9	0.07	6.12	98.9
M-131/10	VV	1.9–146 (33)	62.6	0.01	17.05	99.9
M-131/10-2	VV	3.1–31.0 (32)	11.6	0.23	6.45	96.5
G-9/13	VV	1.9–59.3 (36)	14.4	0.21	5.53	96.3
G-9/13-2	VV	2.2–59.3 (41)	18.5	0.26	5.41	95.5
TPM-1/1	VV	31.5–124 (49)	125.1	5.01	54.59	91.6
Nat-10	VD	1.9–8.2 (38)	5.1	1.21	1.91	61.3
Nat-10-2	VD	2.1–7.9 (35)	4.8	0.42	2.19	83.9
UV-3/13	VD	0.8–5.9 (54)	2.2	0.12	1.30	91.5
VK-2/10	D	1.0–3.2 (29)	2.5	0.04	1.21	96.8
VK-2/10-2	D	0.9–2.9 (10)	2.1	0.56	0.55	49.5
Pyrite						
M-161/10	V	6.9–47.1 (43)	36.3	0.35	17.22	98.1
M-161/10-2	V	2.0–7.4 (27)	4.5	0.18	3.60	95.2
TPM-1/1	VV	1.8–7.9 (30)	6.2	0.32	3.40	91.4
TPM-1/2	VV	1.7–7.6 (19)	5.9	0.33	3.10	90.4
Nat-10	VD	3.1–8.5 (39)	5.3	1.80	2.71	60.0
Nat-10-2	VD	3.1–8.1 (32)	5.5	2.20	1.73	44.0
UV-3/13	VD	1.0–6.0 (52)	2.7	0.29	1.41	82.8
UV-3/13-2	VD	1.3–5.0 (26)	2.6	0.47	1.31	73.7
VK-2/10	D	2.0–3.9 (18)	2.8	0.05	1.10	95.7
VK-2/10-2	D	1.1–2.0 (11)	1.6	0.39	0.37	48.6

Notes: C_{int} is the interval of Au contents in samples (weight 2–5 mg) consisting of "ideal" arsenopyrite and pyrite crystals of different sizes with a well-defined morphological form, the number of analyzed samples (crystals) is given in parentheses; C_{av} is the average Au content in samples; C_{str} is the content of the Au structural form; C_{sur} is the content of the Au surficial form; P_{sur} is proportion of the Au surficial form. For a brief description of the samples from which arsenopyrite and pyrite were taken, see Table 1.

arsenopyrite and pyrite from disseminated ores sampled from slightly altered siltstone shale in the ZDSM: 49.5% and 48.6%, respectively.

4.3. Gold on the surface of arsenopyrite and pyrite crystals

Using the LA-ICP-MS method, the first data were obtained through studies of Au concentrations on the surface of arsenopyrite and pyrite crystals from the highest grade vein and veinlet-vein ores. Two crystals of arsenopyrite (samples M-161/10 and M-131/10) and two crystals of pyrite (samples M-161/10 and TPM-1/1) were analyzed. On the surface of each of these crystals, the laser burned two to three tracks. In order to study the distribution of Au contents with depth, the laser passed along each track six times. In one pass, a layer of 1.0 μm was burned. After six laser passes, the total depth of the tracks was 6.0 μm. The results of the layer-by-layer distribution of Au contents in arsenopyrite and pyrite crystals are shown in Figure 9 and Figure 10. The figures show that the maximum Au concentrations are confined to the surface layer (surface) of 0.0–1.0 μm. With each subsequent laser pass (from 2.0 to 6.0 μm), they gradually decrease. These patterns are

evident in all tracks passed on all four sulfide crystals. The highest Au contents are typical for the surface of arsenopyrite and pyrite crystals from vein ores: up to 92.3 ppm (average is 44.3 ppm) and up to 52.7 ppm (average is 32.1 ppm), respectively (Figures 9a, 10a). Lower Au contents were found on the surface of arsenopyrite and pyrite from veinlet-vein ores: up to 19.8 ppm (average is 17.1 ppm) and up to 18.9 ppm (average is 15.1 ppm), respectively (Figures 9b, 10b).
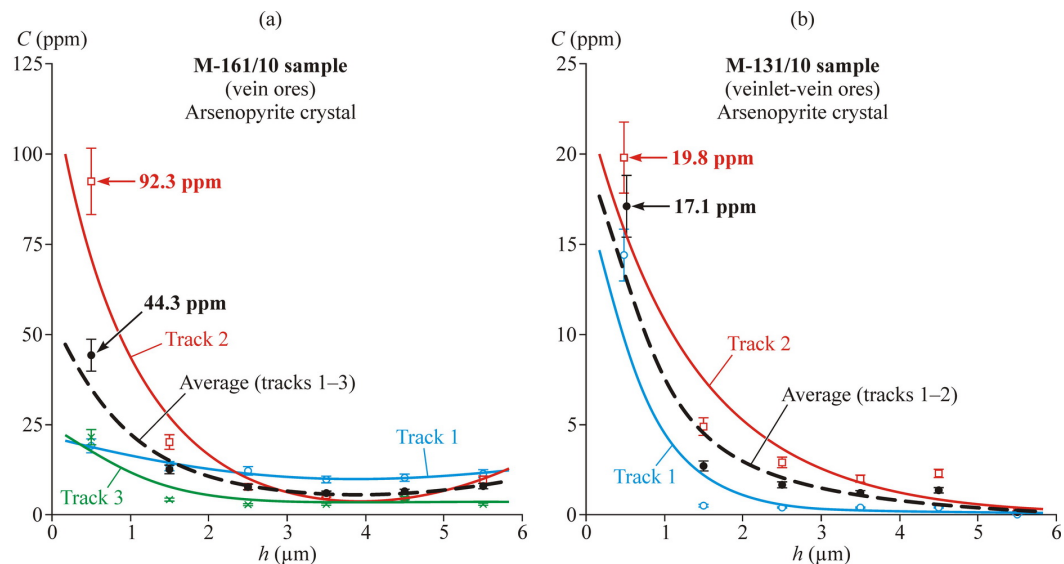
Figure 9. Distribution graphs of average Au contents (C) in surface layers (h) of arsenopyrite crystals taken from samples M-161/10 (a) and M-131/10 (b), according to LA-ICP-MS analysis. Natalka deposit.

9
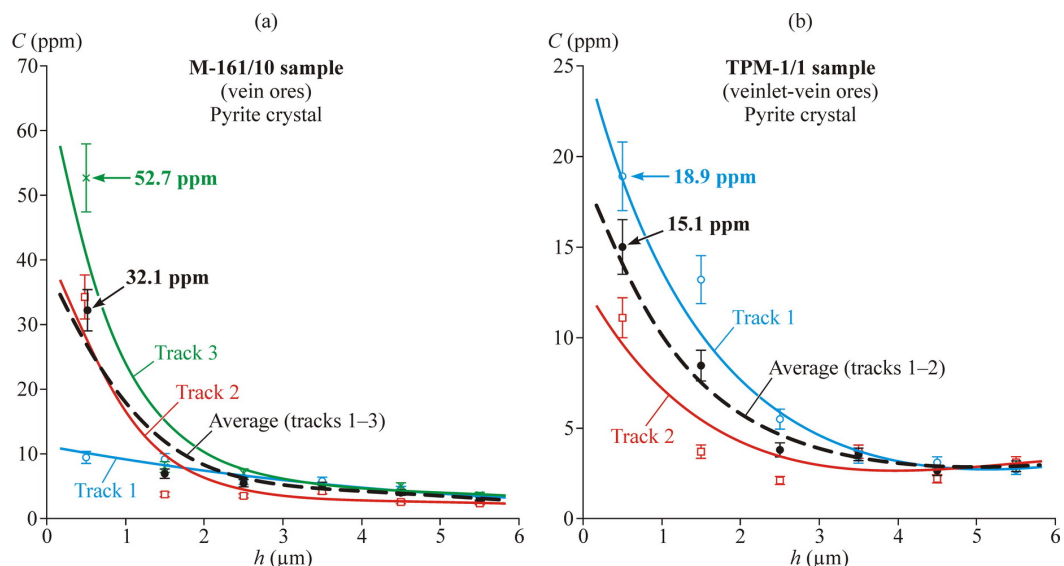
Figure 10. Distribution graphs of average Au contents (C) in surface layers (h) of pyrite crystals taken from samples M-161/10 (a) and TPM-1/1 (b), according to LA-ICP-MS analysis. Natalka deposit.

4.4. Estimation of gold content in ore-forming fluid

When studying the distribution and segregation features of rare trace elements (in our case, gold) during the growth of ore mineral crystals in hydrothermal systems to estimate the Au content in the ore-forming fluid (C_{aq}) of the Natalka and Degdekan (for comparison) orogenic gold deposits, we used the Au content in the structural form in natural pyrite

and the distribution coefficient (D_{str}) for the same form, determined experimentally for hydrothermal systems [*Tauson et al.*, 2011, 2018a, 2019]. The results obtained are presented in Table 3. The maximum Au contents were established in the ore-forming fluid of the Natalka deposit (1.8–22.0 ppm), and the minimum ones were established in the ore-forming fluid of the Degdekan deposit (1.3–2.1 ppm).

Table 3. Comparative assessment of gold content in ore-forming fluid based on pyrite composition of the Natalka and Degdekan gold deposits (North East Russia)

Sample No.	Ore type	N	Au (ppm)		
			C_{str}	C_{sur}	C_{aq}
Degdekan					
DG-10/14	VV	48	0.15	1.31	1.5
DG-10/14-2	VV	44	0.13	1.12	1.3
M-163/10	VD	59	0.21	0.51	2.1
M-163/10-2	VD	45	0.19	0.43	1.9
Natalka					
M-161/10	V	43	0.35	17.22	3.5
M-161/10-2	V	27	0.18	3.60	1.8
TPM-1/1	VV	30	0.32	3.40	3.2
TPM-1/2	VV	19	0.33	3.10	3.3
Nat-10	VD	39	1.80	2.71	18.0
Nat-10-2	VD	32	2.20	1.73	22.0
UV-3/13	VD	52	0.29	1.41	2.9
UV-3/13-2	VD	26	0.47	1.31	4.7

Notes: N is the number of crystals; C_{str} is the content of the Au structural form; C_{sur} is the content of the Au surficial form; C_{aq} is Au content in ore-forming fluid. For gold, the average value of D_{str} is taken to be 0.1 [*Tauson et al.*, 2018a]. The Degdekan gold deposit is located 60 km north of the Natalka deposit and is also orogenic.

5. Discussion

According to the data we obtained (AAS method), the maximum Au contents (ppm) are found in the highest grade vein and veinlet-vein ores: 109.1 (average is 29.2) and 106.9 (average is 27.2), respectively. For veinlet-disseminated ores, lower Au contents are common: no more than 2.90 ppm (average is 1.33 ppm). For poor disseminated ores, which are part of the ore lode and the ZDSM, the maximum Au contents (ppm) are 0.6 (average is 0.11) and 0.19 (average is 0.08), respectively.

According to the PCA-AAS data, not only arsenopyrite, but also pyrite of the Natalka deposit is a gold concentrator (Table 1). The highest contents (ppm) are found in monofractions of arsenopyrite and pyrite from vein ores: up to 1383 (average is 626.1) and up to 250.1 (average is 70.5), respectively. The lowest Au concentrations are typical of disseminated ore sulfides. For arsenopyrite and pyrite from the ores, which are part of the ore lode, the maximum Au concentrations (ppm) are 3.8 (average is 3.1) and 3.4 (average is 2.9), respectively. For pyrite from disseminated ores of the ZDSM, the maximum Au content is 1.7 ppm (average is 1.1 ppm). Arsenopyrite in ZDSM is extremely rare.

Despite the fact that, at present, there is a depletion of the raw material base of easily processed ores, poor disseminated ores of the ZDSM do not cause practical interest in terms of gold mining at the Natalka deposit. In addition, these ores belong to the category of "refractory" ores. However, if we take into account the volume of their occupied areas and the fact that new modern methods of extracting refractory gold from sulfide concentrates already exist, in the future such ores can become a promising source for gold in the mineral resource base of noble metals in Russia. It is important to note that gold mining from disseminated ores is already underway in the Russian North-East at such large deposits as

Degdekan and Pavlik (Magadan region), Mayskoye (Chukotka), Nezhdaninskoye, Badran, Malo-Tarynskoye, Khangalas, Sentachan and Kyuchus (Yakutia). At these deposits, as well as at the Natalka, a significant portion of gold is present in dispersed form in arsenopyrite and pyrite [*Bortnikov et al.*, 2004; *Fridovsky et al.*, 2022; *Genkin et al.*, 1998; *Litvinenko*, 2009; *Moskvitin et al.*, 2023; *Novozhilov and Gavrilov*, 1999; *Sidorova et al.*, 2020, 2022; *Volkov et al.*, 2016].

As was shown previously, in vein, veinlet-vein and veinlet-disseminated ores, the free gold predominates. The main gold carriers are gangue minerals (primarily quartz), and the main concentrators are sulfide minerals [*Goncharov et al.*, 2002; *Goryachkin et al.*, 1999]. The obtained data using LM and EPMA methods, confirm that up to 85% of gold in the Natalka ores is represented by free native gold associated with gangue minerals (primarily quartz, less often feldspars) and ore minerals, the main ones of which are arsenopyrite and pyrite (Figures 3 –7). Gold grains of 0.01 to 2.0 mm in size are prevalent. Up to 20% of gold is finely dispersed particles (< 0.01 mm in size) of native gold, most of which is associated with sulfide minerals (Figures 4–8). The fineness of finely dispersed inclusions is often higher (750–990‰) compared to larger gold (720–860‰). Free gold with an average fineness of 700–850‰predominates (Figure 11).
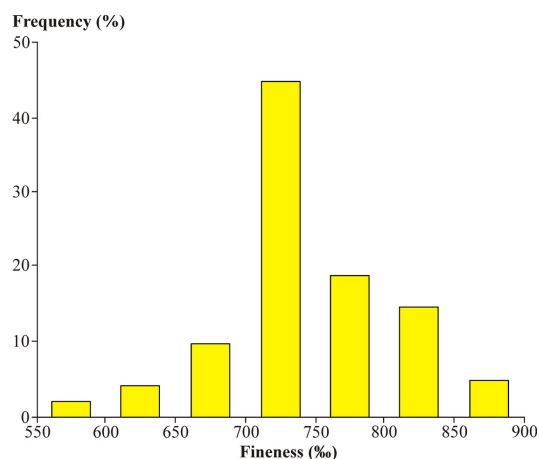
Figure 11. Fineness histogram of free native gold of the Natalka deposit according to [*Savva et al.*, 2022] with minor changes. Number of gold grains is 43.

According to previous researchers [*Goncharov et al.*, 2002], chemical and spectral analysis revealed (in addition to Ag) impurities of Fe, Ti, Al, Sb, As, Hg, Se, Mo, Cu, Pb, Zn, Sn, Bi, Ni and Mn in native gold. The total content of these elements did not exceed 1%. According to [*Savva et al.*, 2022], the quantitative spectral method established impurities of As, Sb, Hg and Pb. At the same time, the As concentrations varied in the range from 0.5 to 18.7 ppm, and the total concentration of all other impurities did not exceed 50 ppm. According to our data, obtained previously using the EPMA method, most of the listed elements are found in native gold in the form of micro-inclusions of their own minerals. The qualitative and quantitative composition of the impurity elements, established by the same method at the present time, is relatively poor. The impurities in gold, in addition to Ag, are often Fe and S only, less common are Bi, As, Hg, Cu and Se, and at single points – W and Pb. These admixtures, being in the invisible mode in native gold for the most part, are probably also represented by proper mineral forms, but only ultra-disperse and nano-dimensional ones (<0.1 µm). It is assumed that W and Sn impurities are usually associated with the influence of granitoids on the geochemical specialization of gold mineralization [*Goncharov et al.*, 2002; *Savva et al.*, 2022; *Volkov et al.*, 2016]. This statement confirms the point of view of researchers who believe that magmatic fluids actively participated in the formation of ores [*Goncharov et al.*, 2002; *Goryachev et al.*, 2008; *Mikhalitsyna and Sotskaya*, 2020; *Savva et al.*, 2022; *Volkov et al.*, 2016].

Earlier, by scanning electron microscopy with energy dispersive X-ray spectrometry (SEM-EDX), we determined the following impurities in one of the gold particles (wt. %): Pt (0.42 to 0.73), Os (0.30 to 0.33), Ir (0.29 to 0.33) and Rh (0.10 to 0.16) [*Kravtsova et al.*, 2020a]. In detail, the distribution features and speciation of platinum group elements in the ores of the Natalka deposit are given in [*Kravtsova et al.*, 2015, 2020b]. It was shown that arsenopyrite and pyrite are the concentrators of not only gold, but also platinoids. The ability to extract these precious metals, primarily Pt, significantly increases the value of the extracted auriferous raw materials. We consider it necessary to emphasize that the study of the platinum-bearing gold deposits and the platinum group elements in the carbonaceous rocks and black-shale strata in general, is currently one of the most promising areas of research, both in Russia and abroad. These deposits are considered to be a new, promising mineral resource by many researchers.

Using the AAS-ADSSC method, in addition to finely dispersed, micron and submicron particles of elemental gold (Au^0), two non-mineral species of "invisible" uniformly distributed gold were found in arsenopyrite and pyrite, namely structural and surficial (Table 2). The structural form corresponds to a chemically-bound element in the mineral structure. The predominant surficial form is confined to nano-sized NAPs and exists in a very thin surface layer of the crystal. The thickness of this layer, according to LA-ICP-MS data (Figures 9, 10), is 0.0–1.0 μm; according to experimental data [*Tauson et al.*, 2009], it is ≤0.5 μm. Gold-rich NAPs are part of the so-called impurity component on the surfaces of arsenopyrite and pyrite crystals. The surficial form proportions of total content of "invisible" gold in sulfides of the ore lode vary in arsenopyrite from 81.8% to 99.9%, in pyrite – from 94.4% to 98.1%. This feature is probably characteristic of the later hydrothermal stages of ore formation. Relatively small proportions of surficially bound gold are found in sulfides of the ZDSM: no more than 49.5% in arsenopyrite and no more than 48.9% in pyrite, which is almost comparable with the proportions of structural gold (Table 2) and is most likely associated with the formation features of the deposit at the early metamorphogenic stage.

Previously conducted SEM-EDX studies of the surface layers of arsenopyrite and pyrite crystals confirmed the presence of high Au content in them [*Kravtsova et al.*, 2020a]. An earlier detailed study of the surface layer of one of the arsenopyrite crystals using the LA-ICP-MS (the maximum track depth for one laser pass was 100 nm, the total pass depth was 600 nm) showed that the maximum average contents of "invisible" Au (23.6 ppm) are characteristic of a thin surface layer of 0–100 nm (Figure 12).

According to previous studies, along with "invisible" gold in the Natalka deposit ores, micro and finely dispersed inclusions of native gold are often developed on the surface and in the surface layers of sulfide crystals taken from ore veins and veinlets [*Kravtsova et al.*, 2020a]. It is assumed that micro and nanoparticles of metallic Au^0 can be formed during post growth transformations of primary nano-sized NAPs. The appearance of micro-mineral forms of native gold in sulfide crystals and within their near-surface layers supports the assumption of partial transformation and directed aggregation of Au-containing nano-sized NAPs [*Tauson et al.*, 2014, 2018b]. As a result, Au^0 particles are formed, ranging from nano- to submicron-sized. This makes it possible to extract such gold during ore beneficiation.

The existence of nano-sized gold in arsenopyrite and pyrite from deposits of different genesis is confirmed by many researchers, but there is no single point of view about its speciation in these minerals [*Ehrig et al.*, 2023; *Fougerouse et al.*, 2016; *Gao et al.*, 2019; *Herrington and Wilkinson*, 1993; *Hough et al.*, 2011; *Kravtsova*, 2010; *Li et al.*, 2019; *Liang et al.*, 2023; *Palenik et al.*, 2004; *Pals et al.*, 2003; *Saunders and Schoenly*, 1995; *Sidorova et al.*, 2020, 2022; *Tauson et al.*, 2011, 2014, 2018b; *Volkov et al.*, 2006]. Although there are many examples, we will only consider a few of them. When studying gold from the Natalka and Mayskoye deposits using the EPMA method, A. V. Volkov and his co-authors came to the conclusion that impurity gold in arsenopyrite exists in the form of nano-sized particles [*Volkov et al.*, 2006]. The existence of "invisible" gold also in the form of an ionic complex (Au^+) and various domain complexes cannot be ruled out. Thus, it is assumed
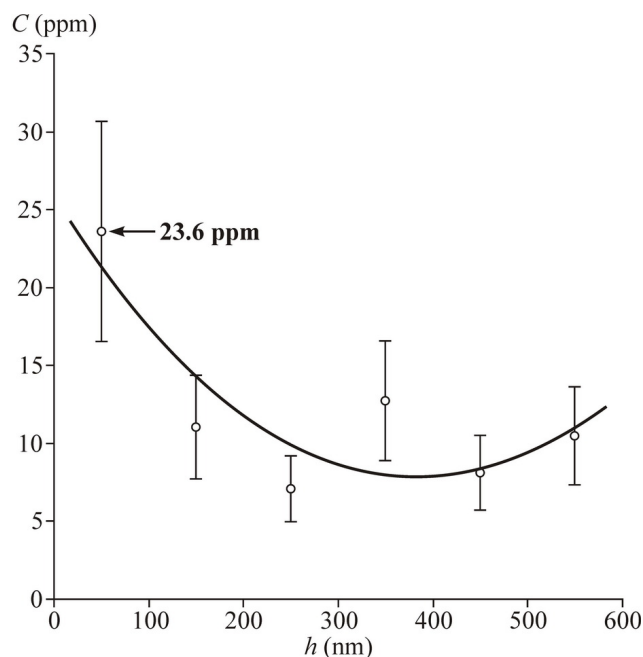
Figure 12. Distribution graph of average Au contents (C) in the surface layers (h) of arsenopyrite crystal (M-129/10 sample) based on LA-ICP-MS data according to [*Kravtsova et al.*, 2015] with minor changes and additions. Natalka deposit.

that the "invisible" gold in the pyrite of the Emperor deposit (Fiji) is included in the pyrite structure as an Au-containing complex. Gold is coordinated as ionic gold (Au^+) [*Pals et al.*, 2003]. According to [*Gao et al.*, 2019], depth profiles obtained by the LA-ICP-MS during the study of trace elements in pyrite of the Huanxiangwa gold deposit (North China) show that "invisible" gold occurs both as solid solution and as homogeneously distributed nanoparticles of native gold, electrum or Au-Ag-Te minerals, as well as in the form of nano- and submicron-sized inclusions of complex Au-Ag-Cu-Pb-Zn domains. According to [*Li et al.*, 2019], at the Baiyun gold deposit (North East China), "invisible" gold in pyrite of an earlier generation exists, in addition to nano-sized or homogeneous inclusions, also in the form of a solid solution. The appearance of visible gold in micro-fractures of later pyrite is thought to be the result of mobilization of earlier nano-sized gold.

Gold nano-sized particles, most importantly, are present not only in sulfide minerals. V. Yu. Prokofiev and co-authors [*Prokofiev et al.*, 2020], while studying drill core of the Kola super-deep borehole SG-3 at a depth of 9052 to 10744 m, found fluid inclusions containing gold nanoparticles in vein quartz. It is assumed that the presence of gold in the form of nano-sized particles in fluids formed during regressive metamorphism of host rocks precedes metamorphic and magmatic fluids that form orogenic gold deposits. It is believed that a significant portion of nano-sized gold can be transported in fluids in the form of colloids in large quantities and that the main concentrators of such gold are sulfides. This point of view is quite widespread [e.g., *Herrington and Wilkinson*, 1993; *Hough et al.*, 2011; *Kravtsova*, 2010; *Saunders and Schoenly*, 1995]. Experimental studies have begun to appear on gold nanoparticles formed on the surface of quartz crystals in the form of submicron islands [*Akimov et al.*, 2024]. All of the above indicates the need to study surficially bound forms of gold not only in sulfide but also in gangue minerals. The relevance of continuing further research in this direction is obvious and important both theoretically and practically.

The structural form of "invisible" gold in the crystals of the sulfides studied, like the surficial form, is also extremely important, even despite its significantly lower concentration compared to the second form (Table 2). It is shown that only data on the content of the structural form of gold in pyrite crystals can be used as an indicator of activity of the

element in a hydrothermal solution [*Tauson et al.*, 2011, 2014]. Our assessment of the Au content in the ore-forming fluid of two orogenic gold deposits located in relative proximity to each other showed that the fluid of the Natalka deposit is enriched in gold (1.8–22.0 ppm) compared to the fluid of the Degdekan deposit (1.3–2.1 ppm). This difference in Au content is consistent with the scope of the two deposits, as the Natalka giant gold deposit is significantly larger in size and gold reserves than the Degdekan deposit (Table 3).

The first data on the study of Au concentrations on the surface of arsenopyrite and pyrite crystals, obtained by the LA-ICP-MS method, confirmed the conclusions obtained by other methods. These data revealed a high degree of enrichment of the surface layer of crystals compared to the matrix: in arsenopyrite up to 92.1 ppm, in pyrite up to 52.7 ppm (Figures 9, 10). That is in principle agreement with the nature of the distribution and concentration levels of "invisible" gold in surface-bound NAPs: up to 54.5 ppm in arsenopyrite and up to 17.2 ppm in pyrite (Table 2). Previous detailed studies have shown that the highest concentrations of "invisible" gold (23.6 ppm), due to NAPs, are confined to the uppermost surface layer of arsenopyrite up to 100 nm deep (Figure 12). It can be assumed that these features are characteristic of not only arsenopyrite, but perhaps represent a general pattern.

6. Conclusions

The generalization and systematization of recent and newly obtained data on the content, distribution and speciation of gold in ores and sulfide minerals of the Natalka deposit are carried out. It is shown that vein and veinlet-vein ores are the highest grade in gold, vein-disseminated ores are the fewer grades, and disseminated ores are poor. According to the AAS data, high average Au contents are found in vein and veinlet-vein ores: 29.2 ppm and 27.2 ppm, respectively. Low average Au contents are common for veinlet-disseminated and disseminated ores, which are part of the ore lode: 1.33 ppm and 0.11 ppm, respectively. For poor disseminated ores of the ZDSM, these contents are the lowest, 0.08 ppm. It has also been established that arsenopyrite is richest in gold, while pyrite is less rich in gold. According to the PCA-AAS data, high average Au contents (ppm) are found in monofractions of arsenopyrite and pyrite from vein ores: 626.1 and 70.5, respectively. Lower average contents (ppm) are typical for arsenopyrite and pyrite from veinlet-vein ores: 42.5 and 8.5, respectively; as well as from veinlet-disseminated ores: 30.2 and 4.6, respectively. Arsenopyrite and pyrite monofractions from disseminated ores of the lode have low average contents: 3.1 ppm and 2.9 ppm, respectively. For pyrites from disseminated ores, which are part of the ZDSM, the maximum average Au content is the lowest, 1.1 ppm.

According to the LM and EPMA data, up to 85% of gold in the vein, veinlet-vein and veinlet-disseminated ores is represented by large and small grains of free native gold associated with gangue (primarily quartz and feldspars) and sulfide minerals. Gold grains of 0.01 to 2.0 mm in size are prevalent. Up to 20% of gold are finely and ultra-dispersed particles (<0.01 mm in size) of native gold. The fineness of such gold is higher (750–990‰) compared to large and small gold (720–860‰). The qualitative and quantitative composition of the impurity elements in native gold is relatively poor. The impurities in gold (in addition to Ag) are often Fe and S only, less common are Bi, As, Hg, Cu and Se. W and Pb are also detected at single points. The presence of W impurities in gold, and according to [*Goncharov et al.*, 2002] also Sn impurities, usually associated with granitoids, confirms the point of view of researchers who believe that magmatic fluids actively participated in the formation of the Natalka ores.

Using the AAS-ADSSC method, in addition to finely dispersed, micron and submicron particles of elemental gold (Au^0), two non-mineral species of "invisible" gold are found in arsenopyrite and pyrite, namely structural and surficial. The first one is incorporated into mineral structure, the second (the predominant one), is confined to nano-sized NAPs on the crystal surface. The first data on the study of Au contents on the surface of arsenopyrite and pyrite crystals, obtained using LA-ICP-MS, confirmed the high degree of enrichment

of the surface layer of crystals compared to the matrix. The proportions of the surficially bound form of gold from the total content of "invisible" gold in sulfides of the ore lode are from 81.8% to 99.9% and from 94.4% to 98.1% in arsenopyrite and pyrite, respectively. Relatively small proportions of surficial gold are found in sulfides of the ZDSM: no more than 49.5% and 48.9% in arsenopyrite and pyrite, respectively. The results obtained by the LA-ICP-MS method are generally comparable with the data established by the AAS-ADSSC method.

We assume that the features revealed by the AAS-ADSSC and LA-ICP-MS methods are closely related to the conditions of the deposit formation, where at the early metamorphogenic stage the proportions of structural gold are almost comparable to the proportions of surficial gold, and at later hydrothermal stages they decreases significantly, to almost complete absence. Along with the "invisible" gold, micron inclusions of native gold are often developed on the surface and within the near-surface layers of sulfide crystals. This is consistent with the model of post-growth transformations of nano-sized NAPs, which lead to the appearance of nano- and submicron Au^0 particles. A comparative assessment of the Au contents in ore-forming fluids of the Natalka and Degdekan orogenic gold deposits, using concentrations of the structural form of gold in natural pyrite and distribution coefficient for the same form, determined experimentally, showed the full importance of this form of gold. Only the structural form of gold makes it possible to conduct comparative assessments of the content of this element in ore-bearing fluids that form gold ore deposits of various composition and genesis and, as a result, to predict the scope of mineralization.

It is assumed that most of the gold contained in arsenopyrite and pyrite as micron- and submicron-sized particles and as surficially bound gold in the form of non-autonomous phases, can be captured with modification of existing flowsheets. To extract the fixed gold, which is in the sulfides as a structural form, the use of more complex technologies is required. Therefore, the need to apply new, modern methods for extracting gold from "refractory" ores is becoming evident. In the long term, this opens up the possibility to involve disseminated ores of the entire mineralized zone in the processing at the Natalka deposit. Taking into account amount of space occupied by such zones, in the future they can become one of the most promising sources for gold in the mineral resources base of noble metals in Russia.

References

Akimov, V. V., D. N. Babkin, and O. Y. Belozerova (2024), Behavior of Gold Nanoparticles at the Interphase Boundary of Quartz-Selenide Copper and Iron at a Temperature of 450 °C and Different Selenium Activity, *Russian Geology and Geophysics*, *65*(8), 910–926, https://doi.org/10.2113/rgg20244691.

Barker, S. L. L., K. A. Hickey, J. S. Cline, et al. (2009), Uncloaking invisible gold: use of nanosims to evaluate gold, trace elements, and sulfur isotopes in pyrite from Carlin-type gold deposits, *Economic Geology*, *104*(7), 897–904, https://doi.org/10.2113/econgeo.104.7.897.

Bortnikov, N. S., I. A. Bryzgalov, N. N. Krivitskaya, et al. (2004), The Maiskoe Multimegastage Disseminated Gold-Sulfide Deposit (Chukotka, Russia): Mineralogy, Fluid Inclusions, Stable Isotopes (O and S), History, and Conditions of Formation, *Geology of Ore Deposits*, *46*(6), 409–440.

Cabri, L. J., S. L. Chryssoulis, J. P. R. De Villiers, et al. (1989), The nature of "invisible" gold in arsenopyrite, *The Canadian Mineralogist*, *27*(3), 353–362.

Cambel, B., V. Streško, and O. Šherenčáaková (1980), The contents of gold in pyrites of various genesis, *Geologický Zbornik - Geologica Carpathica*, *31*(1–2), 139–159.

Cook, N. J., and S. L. Chryssoulis (1990), Concentrations of "invisible gold" in the common sulfides, *The Canadian Mineralogist*, *28*(1), 1–16.

Ehrig, K., C. L. Ciobanu, M. R. Verdugo-Ihl, et al. (2023), Lifting the cloak of invisibility: Gold in pyrite from the Olympic Dam Cu-U-Au-Ag deposit, South Australia, *American Mineralogist*, *108*(2), 259–276, https://doi.org/10.2138/am-2022-8395.

Finkelshtein, A. L., V. V. Tatarinov, E. A. Finkelstein, et al. (2018), About the assessment of gold concentrations in tiny inclusions within sulfide mineral matrix: An electron microprobe study, *X-Ray Spectrometry*, *47*(6), 423–431, https://doi.org/10.1002/xrs.2967.

Fleet, M. E., and A. H. Mumin (1997), Gold-bearing arsenian pyrite and marcasite and arsenopyrite from Carlin Trend gold deposits and laboratory synthesis, *American Mineralogist*, *82*(1–2), 182–193, https://doi.org/10.2138/am-1997-1-220.

Fougerouse, D., S. M. Reddy, D. W. Saxey, et al. (2016), Nanoscale gold clusters in arsenopyrite controlled by growth rate not concentration: Evidence from atom probe microscopy, *American Mineralogist*, *101*(8), 1916–1919, https://doi.org/10.2138/am-2016-5781ccbyncnd.

Fridovsky, V. Y., L. I. Polufuntikova, and M. V. Kudrin (2022), Geochemical and Isotopic Characteristics of Disseminated Sulfide Mineralization of Orogenic Gold Deposits of the Yana-Kolyma Metallogenic Belt, Northeast Russia, *Doklady Earth Sciences*, *507*(S2), S240–S246, https://doi.org/10.1134/s1028334x2260102x.

Gao, F. P., Y. S. Du, Z. S. Pang, et al. (2019), LA-ICP-MS Trace-Element Analysis of Pyrite from the Huanxiangwa Gold Deposit, Xiong'ershan District, China: Implications for Ore Genesis, *Minerals*, *9*(3), 157, https://doi.org/10.3390/min9030157.

Genkin, A. D., N. S. Bortnikov, L. J. Cabri, et al. (1998), A multidisciplinary study of invisible gold in arsenopyrite from four mesothermal gold deposits in Siberia, Russian Federation, *Economic Geology*, *93*(4), 463–487, https://doi.org/10.2113/gsecongeo.93.4.463.

Goncharov, V. I., S. V. Voroshin, and V. A. Sidorov (2002), *Natalka Gold Lode Deposit*, 250 pp., NEISRI FEB RAS (in Russian).

Goryachev, N. A., V. A. Sidorov, I. S. Litvinenko, and T. I. Mikhalitsyna (2000), Mineral composition and petrogeochemical features of ore zones of deep horizons of the Natalka deposit, *Kolyma*, (2), 38–49 (in Russian).

Goryachev, N. A., O. V. Vikent'eva, N. S. Bortnikov, et al. (2008), The world-class Natalka gold deposit, northeast Russia: REE patterns, fluid inclusions, stable oxygen isotopes, and formation conditions of ore, *Geology of Ore Deposits*, *50*(5), 362–390, https://doi.org/10.1134/s1075701508050024.

Goryachkin, N. I., V. A. Chinenov, and V. L. Khoroshilov (1999), Mineralogical characteristics of gold lost during ore processing at the Natalka deposit (North-East of Russia), *Proceedings of higher educational establishments. Geology and Exploration*, (5), 95–102 (in Russian).

Grigorov, S. A., V. D. Vorozhbenko, P. I. Kushnarev, et al. (2007), Geology and key signatures of the Natalka gold deposit, *Domestic Geology*, (3), 43–50 (in Russian), EDN: IAAXZN.

Herrington, R. J., and J. J. Wilkinson (1993), Colloidal gold and silica in mesothermal vein systems, *Geology*, *21*(6), 539–542, https://doi.org/10.1130/0091-7613(1993)021<0539:cgasim>2.3.co;2.

Hough, R. M., R. R. P. Noble, and M. Reich (2011), Natural gold nanoparticles, *Ore Geology Reviews*, *42*(1), 55–61, https://doi.org/10.1016/j.oregeorev.2011.07.003.

Koneev, R. I., R. A. Khalmatov, and A. N. Krivosheeva (2020), Finding forms and Micro- and Nanoscale Assemblages of Gold as Indicators of Formation Conditions, Distribution, and Typification of Orogenic Deposits of Uzbekistan (South Tien Shan), *Geology of Ore Deposits*, *62*(8), 731–742, https://doi.org/10.1134/s1075701520080061.

Kravtsova, R. G. (2010), *Geochemistry and Forming Conditions of Gold-Silver Ore-Forming Systems*, *Northern Pre Okhotsk Region*, 292 pp., Geo, Novosibirsk (in Russian), EDN: QKJONH.

Kravtsova, R. G., and L. A. Solomonova (1985), Gold in Pyrite from Ores and Metasomatites of the Gold-Silver Deposits in the North Okhot'ye Volcanogenic Fields, *Geochemistry International*, *22*(5), 9–14.

Kravtsova, R. G., V. L. Tauson, and E. M. Nikitenko (2015), Modes of Au, Pt, and Pd occurrence in arsenopyrite from the Natalkinskoe deposit, NE Russia, *Geochemistry International*, *53*(11), 964–972, https://doi.org/10.1134/s00167029150 90037.

Kravtsova, R. G., V. L. Tauson, N. A. Goryachev, et al. (2020a), SEM Study of the Surface of Arsenopyrite and Pyrite from the Natalkinskoe Deposit, Northeastern Russia, *Geochemistry International*, *58*(5), 531–538, https://doi.org/10.1134/s0 016702920050031.

Kravtsova, R. G., V. L. Tauson, A. S. Makshakov, et al. (2020b), Platinum Group Elements in Arsenopyrites and Pyrites of the Natalkinskoe Gold Deposit (Northeastern Russia), *Minerals*, *10*(4), 318, https://doi.org/10.3390/min10040318.

Kravtsova, R. G., A. S. Makshakov, V. L. Tauson, et al. (2022), Speciation Features of Gold in Ores And Minerals of the Natalkinskoe Deposit (North-East Russia), *Geodynamics & Tectonophysics*, *13*(2), https://doi.org/10.5800/gt-2022-13-2s-0595 (in Russian).

Large, R. R., and V. V. Maslennikov (2020), Invisible Gold Paragenesis and Geochemistry in Pyrite from Orogenic and Sediment-Hosted Gold Deposits, *Minerals*, *10*(4), 339, https://doi.org/10.3390/min10040339.

Large, R. R., L. Danyushevsky, C. Hollit, et al. (2009), Gold and Trace Element Zonation in Pyrite Using a Laser Imaging Technique: Implications for the Timing of Gold in Orogenic and Carlin-Style Sediment-Hosted Deposits, *Economic Geology*, *104*(5), 635–668, https://doi.org/10.2113/gsecongeo.104.5.635.

Li, C. P., J. F. Shen, S. R. Li, et al. (2019), In-Situ LA-ICP-MS Trace Elements Analysis of Pyrite and the Physicochemical Conditions of Telluride Formation at the Baiyun Gold Deposit, North East China: Implications for Gold Distribution and Deposition, *Minerals*, *9*(2), 129, https://doi.org/10.3390/min9020129.

Liang, Y. Y., L. Shu, P. Y. Ma, et al. (2023), Gold source and ore-forming process of the Linglong gold deposit, Jiaodong gold province, China: Evidence from textures, mineral chemical compositions and sulfur isotopes of pyrite, *Ore Geology Reviews*, *159*, 105523, https://doi.org/10.1016/j.oregeorev.2023.105523.

Litvinenko, I. S. (2009), The conditions of existence and typomorphism of native gold in ores of the Degdekanskoe deposit (northeastern Russia) in black-shale strata, *Russian Geology and Geophysics*, *50*(6), 535–540, https://doi.org/10.1016/j.rgg.2008.10.003.

Liu, J. C., Y. T. Wang, S. K. Huang, et al. (2019), The gold occurrence in pyrite and Te-Bi mineralogy of the Fancha gold deposit, Xiaoqinling gold field, southern margin of the North China Craton: Implication for ore genesis, *Geological Journal*, *55*(8), 5791–5811, https://doi.org/10.1002/gj.3637.

Method NSAM No. 237-S (2016), *Gold Determination in Rocks, Ores and Their Processed Products used Extraction-Atomic-Absorption Method with Organic Sulfides*, 18 pp., VIMS, Moscow (in Russian).

Mikhalitsyna, T. I., and O. T. Sotskaya (2020), The Role of Black-Shale Strata in the Formation of the Natalka and Pavlik Gold Deposits (Yana-Kolyma Orogenic Belt), *Russian Geology and Geophysics*, *61*(12), 1354–1373, https://doi.org/10.15372/rgg2020149.

Moiseenko, V. G., and I. V. Kuznetsova (2010), The role of gold, silver, and lead nanoparticles in the formation of deposits of precious metals, *Doklady Earth Sciences*, *430*(1), 125–128, https://doi.org/10.1134/s1028334x10010277.

Morishita, Y., N. Shimada, and K. Shimada (2018), Invisible gold in arsenian pyrite from the high-grade Hishikari gold deposit, Japan: Significance of variation and distribution of Au/As ratios in pyrite, *Ore Geology Reviews*, *95*, 79–93, https://doi.org/10.1016/j.oregeorev.2018.02.029.

Moskvitin, S. G., L. V. Moskvitina, and V. I. Popov (2023), Morphology and localization of nanoscale gold in the sulphides of the gold-sulphide deposit situated in the black shale strata of the Northern Verkhoyanye in Yakutia, *Tsvetnye Metally*, (3), 13–19, https://doi.org/10.17580/tsm.2023.03.02 (in Russian).

Novozhilov, Y. I., and A. M. Gavrilov (1999), *Gold-sulfide deposits in terrigenous carbonaceous strata*, 220 pp., TsNIGRI, Moscow (in Russian).

Palenik, C. S., S. Utsunomiya, M. Reich, et al. (2004), "Invisible" gold revealed: Direct imaging of gold nanoparticles in a Carlin-type deposit, *American Mineralogist*, *89*(10), 1359–1366, https://doi.org/10.2138/am-2004-1002.

Pals, D. W., P. G. Spry, and S. Chryssoulis (2003), Invisible Gold and Tellurium in Arsenic-Rich Pyrite from theEmperor Gold Deposit, Fiji: Implications for Gold Distribution and Deposition, *Economic Geology*, *98*(3), 479–493, https://doi.org/10.2113/gsecongeo.98.3.479.

Pavlova, L. A. (2014), *The Electron Probe X-Ray Microanalysis and Its Utilization*, 294 pp., LAP LAMBERT Academic Publishing, Saarbrucken (in Russian).

Plyusnina, L. P., A. I. Khanchuk, V. I. Goncharov, et al. (2003), Gold, platinum, and palladium in ores of the Natalka deposit, Upper Kolyma Region, *Doklady Earth Sciences*, *391*(6), 836–340.

Prokofiev, V. Y., D. A. Banks, K. V. Lobanov, et al. (2020), Exceptional Concentrations of Gold Nanoparticles in 1,7 Ga Fluid Inclusions From the Kola Superdeep Borehole, Northwest Russia, *Scientific Reports*, *10*(1), 1108, https://doi.org/10.1038/s41598-020-58020-8.

Saunders, J. A., and P. A. Schoenly (1995), Boiling, colloid nucleation and aggregation, and the genesis of bonanza Au-Ag ores of the sleeper deposit, Nevada, *Mineralium Deposita*, *30*(3–4), 199–210, https://doi.org/10.1007/bf00196356.

Savva, N. E., R. G. Kravtsova, G. S. Anisimova, and G. A. Palyanova (2022), Typomorphism of Native Gold (Geological-Industrial Types of Gold Deposits in the North-East of Russia), *Minerals*, *12*(5), 561, https://doi.org/10.3390/min12050561.

Shao, Y. J., W. S. Wang, Q. Q. Liu, and Y. Zhang (2018), Trace Element Analysis of Pyrite from the Zhengchong Gold Deposit, Northeast Hunan Province, China: Implications for the Ore-Forming Process, *Minerals*, *8*(6), 262, https://doi.org/10.3390/min8060262.

Sidorova, N. V., V. V. Aristov, A. V. Grigor'eva, and A. A. Sidorov (2020), "Invisible" Gold in Pyrite and Arsenopyrite from The Pavlik Deposit (Northeastern Russia), *Doklady Earth Sciences*, *495*(1), 821–826, https://doi.org/10.1134/s1028334x20110136.

Sidorova, N. V., A. V. Volkov, E. V. Kovalchuk, et al. (2022), Invisible Gold and Other Impurity Elements in Pyrite and Arsenopyrite of Disseminated Ores of the Kyuchus Deposit (Sakha Republic (Yakutia)), *Geology of Ore Deposits*, *64*(5), 281–291, https://doi.org/10.1134/s1075701522040067.

Simon, G., S. E. Kesler, and S. Chryssoulis (1999), Geochemistry and textures of gold-bearing arsenian pyrite, Twin Creeks, Nevada; implications for deposition of gold in carlin-type deposits, *Economic Geology*, *94*(3), 405–421, https://doi.org/10.2113/gsecongeo.94.3.405.

Tan, H. J., Y. J. Shao, Q. Q. Liu, et al. (2022), Textures, trace element geochemistry and in-situ sulfur isotopes of pyrite from the Xiaojiashan gold deposit, Jiangnan Orogen: Implications for ore genesis, *Ore Geology Reviews*, *144*, 104843, https://doi.org/10.1016/j.oregeorev.2022.104843.

Tauson, V. L., and E. K. Lustenberg (2008), Quantitative determination of modes of gold occurrence in minerals by the statistical analysis of analytical data samplings, *Geochemistry International*, *46*(4), 423–428, https://doi.org/10.1134/s0016702908040101.

Tauson, V. L., O. I. Bessarabova, R. G. Kravtsova, et al. (2002), Determination of binding forms of gold in pyrite by means of statistical analysis, *Russian Geology and Geophysics*, *43*(1), 56–64.

Tauson, V. L., R. G. Kravtsova, V. I. Grebenshchikova, et al. (2009), Surface typochemistry of hydrothermal pyrite: Electron spectroscopic and scanning probe microscopic data. II. Natural pyrite, *Geochemistry International*, *47*(3), 231–243, https://doi.org/10.1134/s0016702909030021.

Tauson, V. L., D. N. Babkin, T. M. Pastushkova, et al. (2011), Dualistic distribution coefficients of elements in the system mineral-hydrothermal solution. I. Gold accumulation in pyrite, *Geochemistry International*, *49*(6), 568–577, https://doi.org/10.1134/s0016702911060097.

Tauson, V. L., D. N. Babkin, V. V. Akimov, et al. (2013), Trace elements as indicators of the physicochemical conditions of mineral formation in hydrothermal sulfide systems, *Russian Geology and Geophysics*, *54*(5), 526–543, https://doi.org/10.1016/j.rgg.2013.04.005.

Tauson, V. L., R. G. Kravtsova, N. V. Smagunov, et al. (2014), Structurally and superficially bound gold in pyrite from deposits of different genetic types, *Russian Geology and Geophysics*, *55*(2), 273–289, https://doi.org/10.1016/j.rgg.2014.01.011.

Tauson, V. L., S. V. Lipko, N. V. Smagunov, and R. G. Kravtsova (2018a), Trace Element Partitioning Dualism under Mineral-Fluid Interaction: Origin and Geochemical Significance, *Minerals*, *8*(7), 282, https://doi.org/10.3390/min8070282.

Tauson, V. L., S. V. Lipko, N. V. Smagunov, et al. (2018b), Distribution and segregation of trace elements during the growth of ore mineral crystals in hydrothermal systems: geochemical and mineralogical implications, *Russian Geology and Geophysics*, *59*(12), 1718–1732, https://doi.org/10.1016/j.rgg.2018.12.013.

Tauson, V. L., S. V. Lipko, R. G. Kravtsova, et al. (2019), Distribution of "Invisible" Noble Metals between Pyrite and Arsenopyrite Exemplified by Minerals Coexisting in Orogenic Au Deposits of North-Eastern Russia, *Minerals*, *9*(11), 660, https://doi.org/10.3390/min9110660.

Volkov, A. V., A. D. Genkin, and V. I. Goncharov (2006), The forms of the presence of gold in the ores of the Natalka and May deposits (Northeast Russia), *Tikhookeanskaya Geologiya*, *25*(6), 18–29 (in Russian), EDN: JJYBLZ.

Volkov, A. V., A. A. Sidorov, N. E. Savva, et al. (2016), Orogenic Gold Deposits of the Yana-Kolyma Fold Belt: Ore and Fluid Geochemical Peculiarities, Ore Formation Conditions, *The Bulletin of the North-East Scientific Center*, (3), 3–21 (in Russian), EDN: WZWVIV.

Wells, J. D., and T. E. Mullens (1973), Gold-Bearing Arsenian Pyrite Determined by Microprobe Analysis, Cortez and Carlin Gold mines, Nevada, *Economic Geology*, *68*(2), 187–201, https://doi.org/10.2113/gsecongeo.68.2.187.

Zhang, J., J. Deng, H. Y. Chen, et al. (2014), LA-ICP-MS trace element analysis of pyrite from the Chang'an gold deposit, Sanjiang region, China: Implication for ore-forming process, *Gondwana Research*, *26*(2), 557–575, https://doi.org/10.1016/j.gr.2013.11.003.

Zhao, H. X., H. E. Frimmel, S. Y. Jiang, and B. Z. Dai (2011), LA-ICP-MS trace element analysis of pyrite from the Xiaoqinling gold district, China: Implications for ore genesis, *Ore Geology Reviews*, *43*(1), 142–153, https://doi.org/10.1016/j.oregeorev.2011.07.006.